

Chaos and Bifurcation in Roto-Translatory Motion of Gyrostat Satellite

Seyed Mahdi Abtahi ^{1,*}, Seyed Hosein Sadati ²

¹ Department of Mechanical Engineering, Qazvin Branch, Islamic Azad University, Qazvin, Iran

² Department of Mechanical Engineering, Sharif University of Technology, Iran

Received: 15 August 2022- Accepted: 14 November 2022

*Corresponding author: m.abtahi@qiau.ac.ir

Abstract

The chaotic dynamics of Roto-Translatory motion for a triaxial Gyrostat satellite is considered in this study based on the Hamiltonian approach. Higher complexity in the coupled spin-orbit equations motivates the reduction of the Hamiltonian in the study of this nonlinear system. This reduction is done by the use of the Deprit canonical transformation developed here by the new Serret-Andoyer variables used as rotational and translational variables. The results obtained from the Hamiltonian reduction can be written as a perturbed equation near Integrable-Hamiltonian form, where the perturbed part of the equations consists the orbital and gravity gradient effects. Increasing the perturbation parameter causes the trajectories of the system to pass throughout heteroclinic bifurcation zone introducing chaos in the system. Also heteroclinic bifurcation and transversally stable and unstable manifolds are mathematically proven using Melnikov method. Through the Melnikov integral, the bounded variations in the design parameters are determined so as to prevent the system from a chaotic behavior. The simulation results based on the numerical methods such as the time series responses, trajectories of phase portrait, Poincare section, and Lyapunov exponent criterion quantitatively verify chaos in the system in the presence of perturbation influences.

Keywords: Roto-Translatory motion; Gyrostat satellite; Chaotic dynamics; Heteroclinic bifurcation; Melnikov method

1. Introduction

In the recent years, multitude of research works have been done in the general area of chaos present in the chaotic dynamics of pure rotational motion of satellites, though none have looked into the problem of Rotation-Translation together along the orbit. The lack of such research in the Roto-Translatory motion of satellites is more due to the extreme complexity of the motion and the added mathematical burden for the effect of the Gyrostat satellite orbital motion leading to highly coupled equations of motion.

A satellite is mainly a rigid body with a simple dynamic structure. Among the first works in the field of chaotic dynamic analysis of satellites, the paper from Gray et al [1] analyzes the chaotic motion and heteroclinic bifurcation in a rigid body containing internal moving part and viscous damper using Melnikov method, considering the satellite rotational motion only. Bao-Zeng et al [2, 3] studied the chaotic dynamic and heteroclinic bifurcation of a spacecraft with a completely liquid-filled cavity and a satellite with flexible appendage using Melnikov integral. Zhou et al [4] studied the chaos and its stability in a damped satellite filled partially with liquid.

Gyrostat satellites, due to the presence of stabilizers in their dynamic structure, are used in the highly technical missions, resulting in an increase in the complexity of the dynamic modeling. Tong and Tabarrok introduced the analysis of chaotic rotation in the Gyrostat satellite [5]. Kuang et al [6-8] studied the chaotic dynamics of the Gyrostat in spin motion under the gravity gradient torques. They have solved the homoclinic orbits in order to use them in the Melnikov method. Chaotic motion of Kelvin type Gyrostat with one rotor is numerically analyzed by Shirazi and Ghaffari-Saadat [9, 10] using the reduced Hamiltonian equations in their study of chaos. Elip and Lanchares [11] make the solution of the heteroclinic orbits for triaxial Gyrostat with one rotor in terms of elliptic functions. Doroshin [12] analyzed the attitude motion of variable mass coaxial dual-spin Gyrostat satellite, investigating the phase trajectory.

Among limited researches on the Roto-Translatory motion of the satellite, one can point out the work of Celletti et al [13, 14] and Palacian [15] that study the behavior of resonances in the spin-orbit coupling motion in celestial mechanics and measure the basin of attraction of the dynamic system without chaos analysis. Furthermore, there are some publications on the description and application of reduction methods and the procedures for chaos analysis. [16-24]

According to older works, elimination the effects of orbital motion in the attitude dynamics of the Gyrostat system greatly affects the system and it increases the uncertainties between the model and real systems. Therefore, in this work, the Roto-translatory motion of triaxial gyrostat satellite with three rotors as the reaction wheels is modeled under the gravity gradient torques. Newton-Euler approach is initially used to derive the dynamic model of the system. Due to complexity in the coupled equations related to the spin-orbit motion, the Hamiltonian of the system is reduced using the new Serret-Andoyer variables by the developed canonical Deprit transformation. Some numerical and exact mathematical methods are used in the chaos and bifurcation analysis on the reduced equation of motion. Among the numerical methods, time series responses, Poincare section, phase trajectories, and Lyapunov exponent demonstrated the intersection of stable and unstable manifolds in the heteroclinic orbits and chaos phenomenon. In fact, the structure of the governing equations of motion being in near integrable form motivates us to use Melnikov integral for the analysis of chaos and heteroclinic bifurcation mathematically. All these procedures indicate the occurrence of chaos in the system when disturbed by the perturbation. According to the results of Melnikov method, we can determine the bounds corresponding to the variations for the design parameters of the system not resulting in the chaotic motion. In addition, the approach taken in the above analysis also offers an appropriate model for the attitude control of chaos in the satellite system.

2. Mathematical Model of the System

Let us consider the symmetric spacecraft in an equatorial circular orbit under the gravitational field of the earth. In this modeling approach, we focus on the analysis of the attitude dynamics of the Gyrostat satellite along the translational motion. In order to derive the governing equations of motion of the Gyrostat satellite with coupling translational and rotational motion, commonly known as the Roto-translatory motion, we use three different right oriented orthogonal reference frames as follows.

1-The inertia geocentric frame $\mathcal{E} \{X_E, Y_E, Z_E\}$ is used with its origin at the mass center of the earth O_E , the $X_E Y_E$ plane coincides with the equatorial plane, X_E axis passes through the ascending node, and the Z_E axis is aligned with the earth's rotational axes.

2- The orbital frame $\mathcal{R} \{OXYZ\}$ used with its origin at the center of mass of the spacecraft, the Z axis being along the local vertical pointing to the mass center of the earth O_E called the nadir, the Y axis is in the orbital plane coinciding exactly with the velocity vector of the satellite when the satellite is translating along the exact circular orbit, and the X axis is normal to the orbital plane in the direction of the positive angular momentum of the satellite orbital motion. The corresponding unit vectors along these axes are $(\hat{I}, \hat{J}, \hat{K})$ for the roll, pitch, and yaw, respectively.

3- The body frame $\mathcal{B} \{oxyz\}$ coincides with the spacecraft principal axes with their unit vectors $(\hat{i}, \hat{j}, \hat{k})$ aligned with the outward normal to the satellite. (See Fig 1)

The motion of the satellite in the unperturbed state is assumed circular in orbit with null eccentricity, the angular velocity of the satellite around the mass center of the earth is ω_o , and the distance between the mass center of the satellite and earth is R_o . [25, 26]

The gyrostat satellite consists of a rigid main body with three orthogonal planes and three gyros as reaction wheels. The mass of the main body is m_B and the mass of each of the three gyros is m_g . The mass center of the main body without

wheels is G_B and G_i is the mass center of the three gyros ($i = 1,2,3$), with the overall mass center at point G for the gyrostat satellite consisting of the main body along with its three wheels. The reaction wheels are located along the principal axes. So the total inertia tensor of the satellite and its three wheels is diagonal.

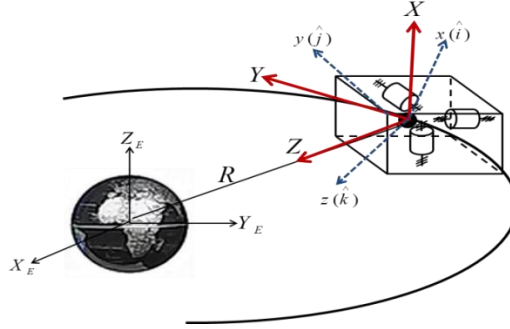


Fig 1- Configuration of Gyrostat and its coordinate systems

The orientation of the two orbital and body frames relative to one another is obtained by means of three Euler angles (φ, θ, ψ) in the sequence $1 \rightarrow 2 \rightarrow 3$ ($x \rightarrow y \rightarrow z$). This classical sequence involves the rotation with φ (roll) about the x axis, followed by the rotation with θ (pitch) about the new y axis, and the last rotation with ψ (yaw) about the new z axis. According to the above assumption, the rotational kinematic model of the satellite is as follows. [25]

$$\begin{aligned}\omega_x &= \dot{\varphi} \cos \psi \cos \theta + \dot{\theta} \sin \psi \\ \omega_y &= \dot{\varphi} \sin \psi \cos \theta + \dot{\theta} \cos \psi \\ \omega_z &= \dot{\psi} + \dot{\varphi} \sin \theta\end{aligned}\quad (1)$$

, where ω_x, ω_y , and ω_z are the angular velocities of the main body expressed in the body frame. The kinematic model of the gyrostat satellite is involving the Euler equation for the rotational motion and the Newton law for the translational motion. In order to derive the Euler equation, we firstly calculate the total angular momentum of the gyrostat satellite related to the overall mass center of the total system (G) as, (see appendix A)

$$\vec{H}_T = (I_{xx}\omega_{xx} + I_W\Omega_x)\hat{i} + (I_{yy}\omega_{yy} + I_W\Omega_y)\hat{j} + (I_{zz}\omega_{zz} + I_W\Omega_z)\hat{k}\quad (2)$$

, where ω_{xx}, ω_{yy} , and ω_{zz} are related to the attitude rotation of the satellite and orbital angular velocity in the body frame as

$$\begin{aligned}\omega_{xx} &= \omega_x + \omega_o \cos \theta \cos \psi \\ \omega_{yy} &= \omega_y - \omega_o \cos \theta \sin \psi \\ \omega_{zz} &= \omega_z + \omega_o \sin \theta\end{aligned}\quad (3)$$

, and Ω_x, Ω_y , and Ω_z are the angular velocities of the reaction wheels relative to the main body with the rotation axes of each gyros aligned with the axes of the body frame. I_{xx}, I_{yy} , and I_{zz} are the inertia elements obtained as

$$\begin{aligned}I_{xx} &= I_x + 3I_W + m_g r^2 (1 + \hat{m}) \\ I_{yy} &= I_y + 3I_W + m_g r^2 (1 + \hat{m}) \\ I_{zz} &= I_z + 3I_W + m_g r^2 (1 + \hat{m})\end{aligned}\quad (4)$$

, where I_x, I_y , and I_z are the inertia momentum of the main body relative to the G_B , I_W is the inertia momentum of each gyro with respect to G_i , r is the distance between the mass center of each gyro and the main body, and $\hat{m} = \frac{m\sqrt{3+3\sqrt{2+(m+2)^2}}}{(m+3)^2}$ where $m = m_B/m_g$ which is derived in the appendix. After derivation of Eq. (2), the Euler equation is expressed as

$$\begin{aligned}
 I_{xx}\dot{\omega}_{xx} + (I_{zz} - I_{yy})\omega_{yy}\omega_{zz} &= N_{cx} + N_{gx} \\
 I_{yy}\dot{\omega}_{yy} + (I_{xx} - I_{zz})\omega_{xx}\omega_{zz} &= N_{cy} + N_{gy} \\
 I_{zz}\dot{\omega}_{zz} + (I_{yy} - I_{xx})\omega_{xx}\omega_{yy} &= N_{cz} + N_{gz}
 \end{aligned}
 \tag{5}$$

, where N_c is the control torques due to the reaction wheels used as the system stabilizer defined as follows

$$\begin{aligned}
 N_{cx} &= -I_W (\dot{\Omega}_x + \omega_{yy}\Omega_z - \omega_{zz}\Omega_y) \\
 N_{cy} &= -I_W (\dot{\Omega}_y + \omega_{zz}\Omega_x - \omega_{xx}\Omega_z) \\
 N_{cz} &= -I_W (\dot{\Omega}_z + \omega_{xx}\Omega_y - \omega_{yy}\Omega_x)
 \end{aligned}
 \tag{6}$$

, and N_{gg} is the gravity gradient perturbation torques on the system given [25]

$$\begin{aligned}
 N_{gg,x} &= \frac{3\mu}{2R_0} (I_{zz} - I_{yy}) \sin 2\varphi \cos^2 \theta \\
 N_{gg,y} &= \frac{3\mu}{2R_0} (I_{zz} - I_{xx}) \sin 2\theta \cos \varphi \\
 N_{gg,z} &= \frac{3\mu}{2R_0} (I_{xx} - I_{yy}) \sin 2\theta \cos \theta
 \end{aligned}
 \tag{7}$$

, where μ is the gravity constant. In order to derive the dynamic equations of translational motion of the satellite, Newton second law is used in the orbital frame, leading to more simplified relations. Neglecting the acceleration of the mass center of the earth with respect to the sun, the orbital equation of motion of the spacecraft is as follows

$$\sum \vec{F} / m_s = (2\dot{R}_0\omega_0 + R_0\dot{\omega}_0)\hat{f} + (R_0\omega_0^2 - \ddot{R}_0)\hat{R}
 \tag{8}$$

, where $\sum \vec{F}$ is the gravity and its perturbed gravity gradient forces. Equations (5) along with equation (8) together describe the coupled dynamic Roto-Translatory motion of the gyrostat satellite.

Performing a simulation of the Newton-Euler model of the system using the shared-memory computing system contain three computational nodes with excessive run time, the trajectory and time series of angular velocities of the system have been obtained and depicted in Fig. 2 and 3, demonstrating quasi periodic-like behavior.

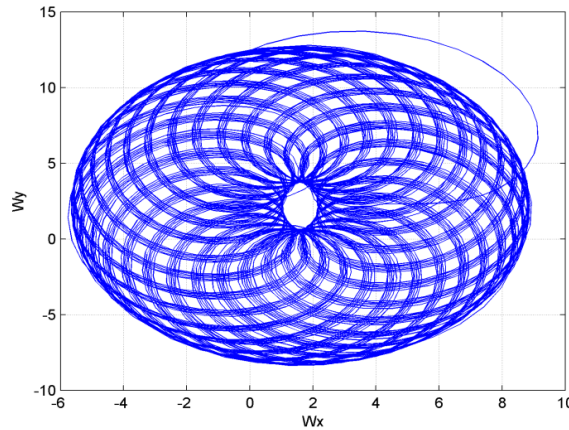


Fig. 2. Trajectory of phase portrait of the system

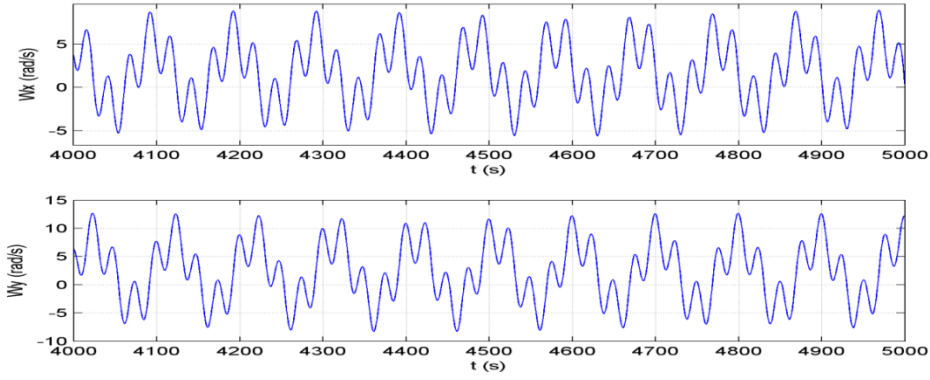


Fig. 3. Time series response of angular velocities of the system

However, due to higher complexity in this modeling, it will be difficult to do much analytical research, making it necessary to obtain a reduced and simpler model so that the reduction method is applied on the Hamiltonian of the system.

3. Hamiltonian of the system

According to the above assumption in the previous section, the kinetic energy of the Roto-Translatory motion of the gyrostat satellite is computed as follows. [26]

$$T = T_{Translation} + T_{Rotation} \quad (9)$$

, where,

$$T_{Translation} = \frac{1}{2} m_B V_{GB}^2 + \frac{1}{2} \sum_{i=1}^3 m_g V_{Gi}^2 \quad (10)$$

, in which V_{GB} is the velocity of the mass center of the main body and V_{Gi} , $i = 1,2,3$ are the components of the velocity of the mass center of each gyro in the three directions, and,

$$\begin{aligned} T_{Rotation} = & \frac{1}{2} \begin{bmatrix} \omega_{xx} & \omega_{yy} & \omega_{zz} \end{bmatrix} \begin{bmatrix} I_x & 0 & 0 \\ 0 & I_y & 0 \\ 0 & 0 & I_z \end{bmatrix} \begin{bmatrix} \omega_{xx} \\ \omega_{yy} \\ \omega_{zz} \end{bmatrix} + \frac{1}{2} \begin{bmatrix} \omega_{xx} + \Omega_x & \omega_{yy} & \omega_{zz} \end{bmatrix} \begin{bmatrix} I_W & 0 & 0 \\ 0 & I_W & 0 \\ 0 & 0 & I_W \end{bmatrix} \begin{bmatrix} \omega_{xx} + \Omega_x \\ \omega_{yy} \\ \omega_{zz} \end{bmatrix} \quad (11) \\ & + \frac{1}{2} \begin{bmatrix} \omega_{xx} & \omega_{yy} + \Omega_y & \omega_{zz} \end{bmatrix} \begin{bmatrix} I_W & 0 & 0 \\ 0 & I_W & 0 \\ 0 & 0 & I_W \end{bmatrix} \begin{bmatrix} \omega_{xx} \\ \omega_{yy} + \Omega_y \\ \omega_{zz} \end{bmatrix} \\ & + \frac{1}{2} \begin{bmatrix} \omega_{xx} & \omega_{yy} & \omega_{zz} + \Omega_z \end{bmatrix} \begin{bmatrix} I_W & 0 & 0 \\ 0 & I_W & 0 \\ 0 & 0 & I_W \end{bmatrix} \begin{bmatrix} \omega_{xx} \\ \omega_{yy} \\ \omega_{zz} + \Omega_z \end{bmatrix} \end{aligned}$$

Simplification of equations (9) to (11) gives the total kinetic energy as follows.

$$\begin{aligned} T = & \frac{1}{2} m_s (\dot{R}_0^2 + R_0^2 \omega_0^2) + \frac{1}{2} \{ I_{2x} \omega_{xx}^2 + I_{2y} \omega_{yy}^2 + I_{2z} \omega_{zz}^2 \} + I_P (\omega_{yy} \omega_{zz} + \omega_{xx} \omega_{zz} + \omega_{xx} \omega_{yy}) + \frac{1}{2} I_W (\Omega_x^2 \\ & + \Omega_y^2 + \Omega_z^2) + I_W (\omega_{xx} \Omega_x + \omega_{yy} \Omega_y + \omega_{zz} \Omega_z) \end{aligned} \quad (12)$$

, where, the first term in the above equation is related to translational motion, and the second and third terms are related to the attitude motion of the spacecraft. The other terms express the kinetic energy of the reaction wheels. The parameters ω_{xx} , ω_{yy} , and ω_{zz} are as given in equation (3). We then have,

$$I_{2x} = I_x + 3I_W + \frac{m_g r^2}{m_s} (2m_g + m_B) \quad (13)$$

$$I_{2y} = I_y + 3I_W + \frac{m_g r^2}{m_s} (2m_g + m_B)$$

$$I_{2z} = I_z + 3I_W + \frac{m_g r^2}{m_s} (2m_g + m_B)$$

, and

$$I_P = \frac{m_g^2 r^2}{m_s} \quad (14)$$

, where m_s denotes the whole mass of the gyrostat satellite expressed as $m_s = m_B + 3m_g$. According to the gravitational field of the earth, the potential energy of the spacecraft is derived as,

$$U_g = -\frac{GMm_s}{R_0} \quad (15)$$

, where, G is the universal gravity constant and M is the mass of the earth. In order to derive the equation of motion of the system by means of the Hamiltonian method, the Lagrangian of the spacecraft is first calculated as follows.

$$L = T - U_g = L(q_i, \dot{q}_i) \quad (16)$$

, where, q_i 's are the generalized coordinates describing the Roto-Translatory motion, which involves the rotational coordinates (φ, θ, ψ) and orbital coordinates (μ_o, R_o) with the μ_o being similar in concept to the definition of eccentric anomaly in the astronomy and defined by $\omega_o = \frac{d}{dt}\mu_o = \dot{\mu}_o$. In this modeling approach, the orbital motion of the spacecraft is assumed planar and only two coordinates are allocated to the translational motion. The relations between the generalized coordinates (q_i) and the angular velocities in equation (12) are expressed by the kinematic model described by equations (1) and (3). Consequently, the generalized momentum related to each generalized coordinates is derived as follows.

$$P_\varphi = \frac{\partial L}{\partial \dot{\varphi}}, \quad P_\theta = \frac{\partial L}{\partial \dot{\theta}}, \quad P_\psi = \frac{\partial L}{\partial \dot{\psi}}, \quad P_{\mu_o} = \frac{\partial L}{\partial \dot{\mu}_o}, \quad P_{R_o} = \frac{\partial L}{\partial \dot{R}_o} \quad (17)$$

Using the Legendre transformation, the Hamiltonian of the system is then obtained as

$$H = \dot{\varphi}P_\varphi + \dot{\theta}P_\theta + \dot{\psi}P_\psi + \dot{\mu}_o P_{\mu_o} + \dot{R}_o P_{R_o} - L \quad (18)$$

It is noted that the determination of the above Hamiltonian and its related equations of motion are quite complex. Since the order of magnitudes of ω_o^2 and $1/R_o^2$ in the translational motion are insignificant compared to those of the other coordinates, we can write the kinetic energy in the control torque-free case in the following simple form as

$$T = T_0(q_i, \dot{q}_i) + \omega_o T_1(q_i, \dot{q}_i) + \omega_o^2 T_2(q_i) \quad (19)$$

, in which

$$T_0 = \frac{1}{2} [\omega_x \quad \omega_y \quad \omega_z] [\tilde{I}] [\omega_x \quad \omega_y \quad \omega_z]^T + \frac{1}{2} m_s R_o^2 \omega_o^2 + \frac{1}{2} m_s \dot{R}_o^2 \quad (20)$$

$$T_1 = \frac{1}{2} [C_\theta C_\psi \quad -C_\theta S_\psi \quad S_\theta] [\tilde{I}] [\omega_x \quad \omega_y \quad \omega_z]^T \quad (21)$$

$$T_2 = \frac{1}{2} [C_\theta C_\psi \quad -C_\theta S_\psi \quad S_\theta] [\tilde{I}] [C_\theta C_\psi \quad -C_\theta S_\psi \quad S_\theta]^T \quad (22)$$

, where

$$\tilde{I} = \begin{bmatrix} I_x & I_P & I_P \\ I_P & I_y & I_P \\ I_P & I_P & I_z \end{bmatrix}$$

, and $C_{(\cdot)} \triangleq \cos(\cdot)$ and $S_{(\cdot)} \triangleq \sin(\cdot)$, also using equations (15) and (19), the Hamiltonian in the new form is obtained by the Legendre transformation as

$$H = \{\dot{\varphi}P_\varphi + \dot{\theta}P_\theta + \dot{\psi}P_\psi + \dot{\mu}_0 P_{\mu_0} + \dot{R}_0 P_{R_0}\} - \{T_0 + (\omega_0)T_1 + (\omega_0^2)T_2 - U_g\} \quad (23)$$

According to equation (19), the first part of the above Hamiltonian is simplified, which is then written in the form [9]

$$H = T_0 + (\omega_0)T_1 + (\omega_0^2)T_2 + U_g \quad (24)$$

Using the principal axes of coordinate system (xx, yy, zz) , the matrices in equations (20) to (22) becomes diagonal with the rotation matrix whose columns involve the eigenvectors of original matrix. Therefore, the Hamiltonian of the system in the new principal coordinates is obtained as

$$H_n = H_0 + (\omega_0)H_1 + (\omega_0^2)H_2 \quad (25)$$

, and

$$H_0 = \frac{1}{2}I_{xx}\omega_{xx}^2 + \frac{1}{2}I_{yy}\omega_{yy}^2 + \frac{1}{2}I_{zz}\omega_{zz}^2 + \frac{1}{2}(m_s R_0^2)\omega_0^2 + \frac{1}{2}m_s \dot{R}_0^2 + \frac{GMm_s}{R_0} \quad (26)$$

$$H_1 = I_{xx}C_\theta C_\psi \omega_{xx} - I_{yy}C_\theta S_\psi \omega_{yy} + I_{zz}S_\theta \omega_{zz} \quad (27)$$

$$H_2 = \frac{1}{2}I_{xx}C_\theta^2 C_\psi^2 - \frac{1}{2}I_{yy}C_\theta^2 S_\psi^2 + \frac{1}{2}I_{zz}S_\theta^2 \quad (28)$$

, where H_n is the Hamiltonian in the principal coordinate of the inertia tensor \tilde{I} , which is defined under equation (22), ω_{xx} , ω_{yy} and ω_{zz} are the angular velocity components of the satellite along the principal axes of \tilde{I} , and I_{xx} , I_{yy} , and I_{zz} are the principal inertia momentum of the Gyrostat satellite equivalent to the eigenvalues of \tilde{I} . The (Φ, Θ, Ψ) are the new set of Euler angles in the direction of the principal axes of \tilde{I} , coinciding with the (φ, θ, ψ) angles after transformation to new principal coordinates. The generalized momentum based on the Hamiltonian of the system using the new coordinate (Φ, Θ, Ψ) are computed using equations (17).

$$P_\Phi = (I_{xx}C_\theta C_\psi)\omega_{xx} - (I_{yy}C_\theta S_\psi)\omega_{yy} + (I_{zz}S_\theta)\omega_{zz} + (I_{xx}C_\theta^2 C_\psi^2 + I_{yy}C_\theta^2 S_\psi^2 + I_{zz}S_\theta^2)\omega_0 \quad (29)$$

$$P_\Theta = (I_{xx}S_\psi)\omega_{xx} + (I_{yy}C_\psi)\omega_{yy} + (I_{xx}C_\theta C_\psi S_\psi - I_{yy}C_\theta S_\psi)\omega_0 \quad (30)$$

$$P_\Psi = (I_{zz})\omega_{zz} + (I_{zz}S_\theta)\omega_0 \quad (31)$$

$$P_{\mu_0} = (I_{xx}C_\theta C_\psi)\omega_{xx} - (I_{yy}C_\theta S_\psi)\omega_{yy} + (I_{zz}S_\theta)\omega_{zz} + (m_s R_0^2 + I_{xx}C_\theta^2 C_\psi^2 - I_{yy}C_\theta^2 S_\psi^2 + I_{zz}S_\theta^2)\omega_0 \quad (32)$$

$$P_{R_0} = (m_s)\dot{R}_0 \quad (33)$$

Equations (29) to (33) will now be used to solve for the generalized velocities with respect to the generalized momentum variables. Using these results then, the Hamiltonian in equation (24) is written in the form

$$H_n = H_{up} + \varepsilon_1 H_{p1} + \varepsilon_2 H_{p2} \quad (34)$$

, where

$$H_{up} = \frac{P_\Psi^2}{2I_{zz}} + \frac{P_{R_0}^2}{2m_s} + P_\Theta^2 \left(\frac{C_\psi^2}{2I_{yy}} + \frac{S_\psi^2}{2I_{xx}} \right) + \frac{GMm_s}{R_0} + \left(\frac{P_\Phi}{C_\theta} - P_\Psi \tan\theta \right)^2 \left(\frac{C_\psi^2}{2I_{xx}} + \frac{S_\psi^2}{2I_{yy}} \right) + \left(\frac{P_\Phi}{C_\theta} - P_\Psi \tan\theta \right) P_\Theta S_\psi C_\psi \left(\frac{1}{I_{xx}} - \frac{1}{I_{yy}} \right) \quad (35)$$

$$H_{p1} = \frac{1}{2}I_{xx}C_\theta^2 C_\psi^2 - \frac{1}{2}I_{yy}C_\theta^2 S_\psi^2 + \frac{1}{2}I_{zz}S_\theta^2 \quad (36)$$

$$H_{p2} = 2P_\Phi P_\Psi S_\theta - 4P_\Phi P_\Psi S_\theta S_\psi^2 + \frac{(P_\Phi - P_{\mu_0})^2}{2} - P_\Phi^2 S_\psi^2 \quad (37)$$

, with $\varepsilon_1 = \omega_0^2$ and $\varepsilon_2 = 1/m_s R_0^2$. In equation (34), the Hamiltonian for the torque-free motion is written in the form of a complete integrable term H_{up} and two other perturbation terms H_{p1} and H_{p2} which are related to the parameters consisting of the orbital angular velocity ε_1 and the orbital radius vector of the satellite ε_2 .

There are some salient points of importance according to equations (34) to (37). Among them, it is noted that the derivation of the Hamiltonian in the form of Eq. (34) helps to use the perturbation method to analyze the system. It is also evidence that the effect of the translational motion of the satellite is much less than that of the rotational ones. This indicated that the relative rotational energy is quite larger than the translational energy. Furthermore, the integrability and regularity of the rotational motion is increased. One important point noted in the above Hamiltonian is its extreme complexity, making the system analysis quite difficult. On the other hand, finding some "constant of motion" in the system can reduce the Hamiltonian to a simple form. This is done by means of the new Deprit transformation.

4. Reduction of Hamiltonian using new Deprit Transformation

Considering the Hamiltonian obtained in the previous section, since the coordinate Φ does not directly appear in the Hamiltonian equation, Φ is a cyclic coordinate. Therefore, the generalized momentum P_ϕ related to this cyclic coordinate is an integral of motion, making it one of the constants of motion. It indicates the possibility of system reduction to a system with exactly one less degree of freedom using a proper canonical transformation. This reduction is done with the help of the Deprit canonical transformation by defining the new Serret-Andoyer variables for the Roto-Translatory motion to transform the old variables to the new ones according to the spherical triangle shown in Fig. 4 and its related. [16-18]

The old variables are

$$\{\Phi, \Theta, \Psi, \mu_O, R_O, P_\phi, P_\Theta, P_\Psi, P_{\mu_O}, P_{R_O}\}$$

, and the new variables under transformation are

$$\{h, g, l, \lambda_O, r_O, P_h, P_g, P_l, P_{\lambda_O}, P_{r_O}\}$$

The new Serret-Andoyer relations of transformation are defined as follows.

$$P_\Phi = P_h \tag{38}$$

$$P_\Theta = P_g S_j S_{\Psi-1} \tag{39}$$

$$P_\Psi = P_l \tag{40}$$

$$P_{\mu_O} = P_{\lambda_O} \tag{41}$$

$$P_{R_O} = P_{r_O} \tag{42}$$

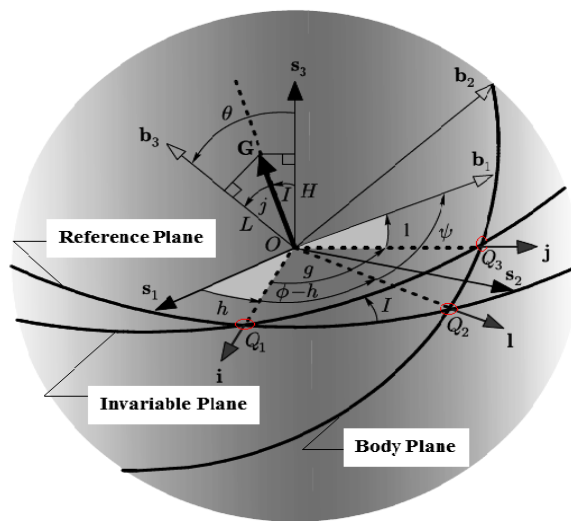


Fig. 4. Definition of Serret-Andoyer variables in Deprit Transformation [16]

Equations (38) to (40) are related to the rotational motion and equations (41) and (42) correspond to the translational motion. Then the relations based on the spherical triangle $Q_1Q_2Q_3$ are as follows [16, 27].

$$\cos(\Theta) = \cos(I) \cos(J) - \sin(I)\sin(J)\cos(g) \quad (43)$$

$$\cos(\Psi - l) = \cos(\Phi - h) \cos(g) + \sin(\Phi - h)\sin(g) \cos(I) \quad (44)$$

$$\cos(\Phi - h) = \cos(\Psi - l) \cos(g) + \sin(\Psi - l)\sin(g) \cos(J) \quad (45)$$

, where,

$$\cos(I) = \frac{P_h}{P_g} \quad \cos(J) = \frac{P_l}{P_g} \quad (46)$$

Substituting equations (43) to (46) and their results into equations (34) to (37), the reduced Hamiltonian in its simplest form here is obtained as

$$H'_n = H'_{up} + \varepsilon_1 H'_{p1} + \varepsilon_2 H'_{p2} \quad (47)$$

, where

$$H'_{up} = \frac{P_l^2}{2I_{zz}} + \frac{P_{r_o}^2}{2m_s} + \frac{GMm_s}{r_o} + \frac{1}{2}(P_g^2 - P_l^2) \left(\frac{S_l^2}{I_{xx}} + \frac{C_l^2}{I_{yy}} \right) \quad (48)$$

$$H'_{p1} = \frac{1}{2} \{ I_{zz} - I_{zz}C_l^2C_g^2 - I_{zz}S_l^2S_g^2C_g^2 + \frac{1}{2}(I_{zz} - I_{xx})S_{2l}S_{2j} + (I_{xx} - I_{yy})(S_l^2S_jC_g + C_lS_jC_l) - I_{xx}S_j^2 + I_{yy}C_l^2S_g \} \quad (49)$$

$$H'_{p2} = \frac{1}{2}P_{\lambda_o}^2 + P_{\lambda_o} \left(S_j^2S_l^2 + \frac{1}{2}S_{2l}C_{2j} \right) + P_l(S_l^2S_j + S_lS_gS_l) + S_gC_l + S_l^2 - S_lS_j \quad (50)$$

Consequently, the canonical equations of motion based on the reduced Hamiltonian of the system using generalized coordinates and momentum in the absence of the external control torques are evaluated as follows.

$$\dot{h} = \frac{\partial H'_n}{\partial P_h} = 0 \quad (51)$$

$$\dot{g} = \frac{\partial H'_n}{\partial P_g} = P_g \left(\frac{S_l^2}{I_{xx}} + \frac{C_l^2}{I_{yy}} \right) \quad (52)$$

$$\dot{l} = \frac{\partial H'_n}{\partial P_l} = P_l \left(\frac{1}{I_{zz}} - \frac{S_l^2}{I_{xx}} - \frac{C_l^2}{I_{yy}} \right) + \varepsilon_2(G_{l2}) \quad (53)$$

$$\dot{\lambda}_o = \frac{\partial H'_n}{\partial P_{\lambda_o}} = 0 + \varepsilon_2(G_{\lambda_o2}) \quad (54)$$

$$\dot{r}_o = \frac{\partial H'_n}{\partial P_{r_o}} = \frac{1}{m_s}P_{r_o} \quad (55)$$

$$\dot{h} = -\frac{\partial H'_n}{\partial h} = 0 + \varepsilon_g(N_{gg,h}) \quad (56)$$

$$\dot{g} = -\frac{\partial H'_n}{\partial g} = 0 + \varepsilon_1(G_{Pg1}) + \varepsilon_2(G_{Pg2}) + \varepsilon_g(N_{gg,g}) \quad (57)$$

$$\dot{l} = -\frac{\partial H'_n}{\partial l} = -(P_g^2 - P_l^2)S_lC_l \left(\frac{1}{I_{xx}} - \frac{1}{I_{yy}} \right) + \varepsilon_1(G_{Pl1}) + \varepsilon_2(G_{Pl2}) + \varepsilon_g(N_{gg,l}) \quad (58)$$

$$\dot{\lambda}_o = -\frac{\partial H'_n}{\partial \lambda_o} = 0 \quad (59)$$

$$\dot{r}_o = -\frac{\partial H'_n}{\partial r_o} = \frac{GMm_s}{R_o^2} \quad (60)$$

, where $\varepsilon_g = 3\mu/2r_o^3$ is the perturbation parameter of the gravity gradient torques and N_{gg} is the gravity gradient torques based on equation (7) after transformation by Serret-Andoyer variables, and we have

$$G_{l2} = S_l^2S_j + S_lS_gS_l$$

$$\begin{aligned}
G_{\lambda_0 2} &= S_f^2 S_l^2 + \frac{1}{2} S_{2l} C_{2j} + P_{\lambda_0} \\
G_{P_g 1} &= -I_{zz} S_l^2 S_f^2 S_g C_g + \frac{1}{2} (I_{xx} - I_{yy}) S_l^2 S_j S_g - \frac{1}{2} I_{yy} C_l^2 C_g \\
G_{P_g 2} &= -P_l (S_l C_g S_l) - C_g C_l \\
G_{P_l 1} &= \frac{1}{2} (I_{xx} - I_{yy}) C_l S_j S_l \\
G_{P_l 2} &= S_g S_l - P_l S_l S_g C_l
\end{aligned}$$

According to the equations (51-60) in the unperturbed and torque free system, we have two constant parameter named h, λ_0 and two integral of motion due to be zero the value of P_h, P_{λ_0} . As a result, using the new Deprit transformation, the system with order of 5 is reduced to the system with order of 3 in the unperturbed system.

5. Numerical Analysis of Chaos

The reduced Hamiltonian in the previous section can be used for a thorough and precise analysis study on the nonlinear system. Since the translational motion of the gyrostat satellite affects through perturbation terms, the rotational motion of the system dynamics is considered to be the more essential part, expressed by equations (53) and (58) rewritten as follows.

$$\dot{l} = P_l \left(\frac{1}{I_{zz}} - \frac{S_l^2}{I_{xx}} - \frac{C_l^2}{I_{yy}} \right) + \varepsilon(G_l) \quad (61)$$

$$\dot{P}_l = -(P_g^2 - P_l^2) S_l C_l \left(\frac{1}{I_{xx}} - \frac{1}{I_{yy}} \right) + \varepsilon(G_{P_l}) \quad (62)$$

, where $\varepsilon = 1/r_0^2$ is a unique perturbation parameter consisting of $\varepsilon_1, \varepsilon_2, \varepsilon_g$ and,

$$\begin{aligned}
G_l &= \frac{1}{m_s} \{ S_f^2 S_j + S_l S_g S_l \} \\
G_{P_l} &= v_0^2 \left\{ \frac{1}{2} (I_{xx} - I_{yy}) C_l S_j S_l \right\} + \frac{1}{m_s} \{ S_g S_l - P_l S_l S_g C_l \} + \frac{2\mu}{3r_0} \{ S_h S_g C_l^2 - 2S_j C_l C_h^2 \}
\end{aligned}$$

, and v_0 is the orbital velocity of the spacecraft. According to equations (61) and (62), the unperturbed system ($\varepsilon = 0$) has five fixed points based on the values of inertia moments. The fixed point (0,0) is hyperbolic saddle point corresponding to the spin about the intermediate axis (yy), and the two equilibrium points $(\pm \frac{\pi}{2}, 0)$ are on the border of stability margin corresponding to the spin around the minor (zz) and major (xx) axes, respectively. The fixed points $(\sin^{-1} \sqrt{\frac{I_{xx} - I_{yy} - I_{zz}}{I_{yy} - I_{zz}}}, \pm P_g)$ are related to the upper and lower limits of the phase portrait which are beyond the region of interest.

In order to numerically analyze the dynamical system, the equations of motion in (51) through (60) are simulated using the Range-Kutta method. The procedure for the Poincare map is then used to study the nonlinear system for $I_{xx} > I_{yy} > I_{zz}$. The Poincare map of the system is generated by intersecting the trajectories of the phase portrait with plane $g = \pi$ in mod 2π . The Poincare section of the system is demonstrated in Fig. 5 in the unperturbed case ($\varepsilon = 0$) for $I_{xx} = 1.8$, $I_{yy} = 1.2$, $I_{zz} = 0.8$, and $P_h = 0.7$. This figure clearly shows the regularity in the unperturbed system. The Poincare section of the perturbed system under the translational effects and gravity gradient torques is demonstrated in Fig. 6.

According to the intersection of stable and unstable manifolds in the heteroclinic orbits in Poincare plane, the chaotic behavior can occur in the system. Based on the Smale-Birkhoff theorem, heteroclinic intersection in Poincare plane can

describe the behavior of the system by a horseshoe map. When a heteroclinic intersection occurs, one trajectory on the unstable manifold joins another trajectory on the stable manifold.

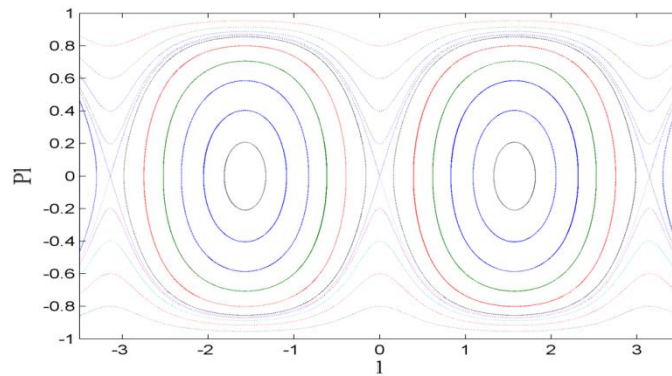


Fig. 5. Regular Poincaré section of the unperturbed system for $\varepsilon = 0$

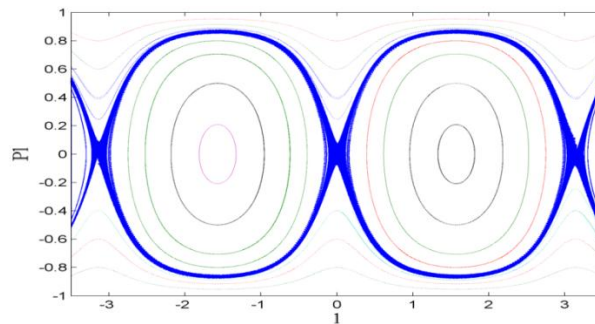


Fig. 6. chaotic Poincaré section of the perturbed system for $\varepsilon = 2 \times 10^{-8}$

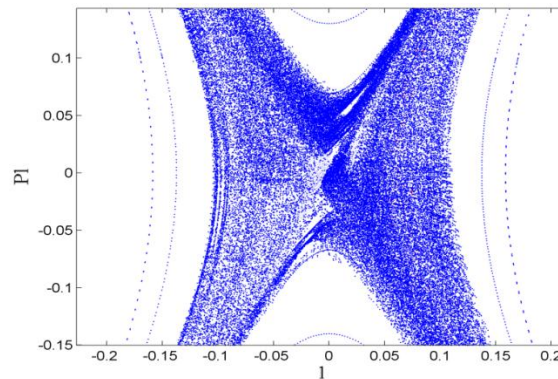


Fig. 7. Poincaré section and chaotic band near the saddle point for $\varepsilon = 2 \times 10^{-8}$

In fact, a trajectory near the saddle point approaches to it by the stable manifold, and that trajectory is then forced away from a saddle point by the unstable manifold. Hence, a heteroclinic tangling is developed around the saddle point and the trajectories can seem to wander randomly near the saddle point, introducing a basin of attraction in some dissipative systems. Stated differently, the stretching, compression, and folding in the trajectories of the system around the saddle points are actually influenced by the heteroclinic intersection. Therefore, it shows a horseshoe map behavior and ultimately a heteroclinic tangling may show chaotic trajectories. According to Fig. 7, a chaotic behavior appears near the saddle point, where the chaotic band with chaos windows is shown in the figure clearly. [23, 24]

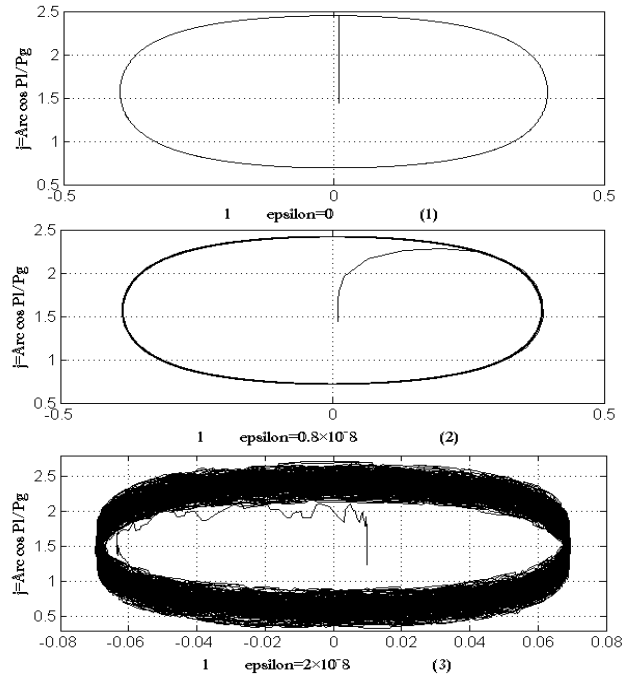


Fig. 8. Growth of the irregularity of the system with increase in ϵ

Another procedure for chaos analysis is the global heteroclinic bifurcation that shows the effects of perturbation on the system. As Fig. 8 shows, the variation of phase portrait of the system is demonstrated with respect to the changes of the perturbation parameter. Fig 8(1) is related to the unperturbed system ($\epsilon = 0$) which includes a regular stable limit cycle with periodic behavior. However, increasing the perturbation parameter causes to intensify the irregularity in the limit cycle and as in Fig. 8(2), the dynamics of the system is similar to a quasi-periodic manner. Finally, based on the true value of the perturbation parameter ($\epsilon = 2 \times 10^{-8}$) as shown in Fig. 8(3), the behavior of the system will become like a chaotic system.

One of the strong tools for numerical analysis of a chaotic system is the Lyapunov exponent method. The Lyapunov exponent measures exponentially the attraction or divergence of two adjacent orbits in time in the phase space with close initial conditions. Furthermore, the Lyapunov exponent displays the sensitivity of the system to initial condition. The Lyapunov exponent (λ) for each state variable ($x_i(t)$) is mathematically defined as

$$\lambda = \lim_{t \rightarrow \infty} \frac{1}{t} \int_0^t E_i(x(\tau)) d\tau = \lim_{t \rightarrow \infty} \frac{1}{t} \ln \left| \frac{\delta x_i(t)}{\delta x_i(0)} \right| \tag{63}$$

, where, $x_i(0)$ is the initial condition, and $E_i(x(t))$ is the real eigenvalue of the Jacobian matrix related to the divergence rate of the system. Therefore, if the largest Lyapunov exponent is negative, then the orbits converge together and, if it is positive, then the distance between the adjacent orbits grows exponentially and the system exhibits sensitively dependence on the initial condition. As a result, if the system has at least one positive Lyapunov exponent, it usually indicates chaos [21, 24].

In this section, after calculation of the Lyapunov exponent for each state, the diagram for the largest Lyapunov exponent with respect to the increase in the perturbation parameter is obtained. According to Fig. 9, increasing the perturbation parameter of the system results in a Lyapunov exponent sign change to positive, which in turn increases the possibility of chaos in the system. The results shown in Fig. 9 completely agree with those of the heteroclinic bifurcation diagram of Fig. 8.

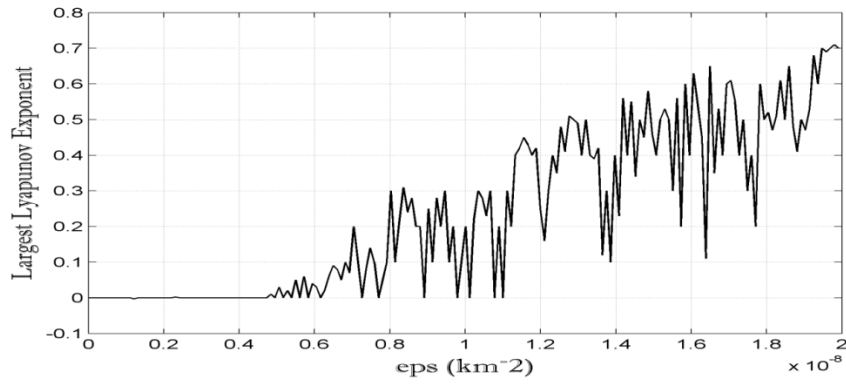


Fig. 9. Largest Lyapunov exponent of the system with increasing the ϵ

Simulation results of the system are obtained under the initial condition $h_0 = 0.5, g_0 = 0.1, l_0 = 0.01, \lambda_{0_0} = 1.1, r_{0_0} = 6675,$ and $P_{h_0} = 0.3, P_{g_0} = 0, P_{l_0} = 0, P_{\lambda_{0_0}} = 0, P_{r_{0_0}} = 1.4.$ Poincare section and trajectories of the system demonstrate a total chaotic behavior in the perturbed system. For instance, the Poincare section of the system that includes the intersection of $l - I - J$ trajectory of the system with the plane $l = \pi/2$ in mod 2π is shown in Fig. 10, verifying the chaotic behavior in the system. In addition, the trajectories of the system under the above initial condition are demonstrated in Figs. (11) to (13), again indicating chaotic behavior.

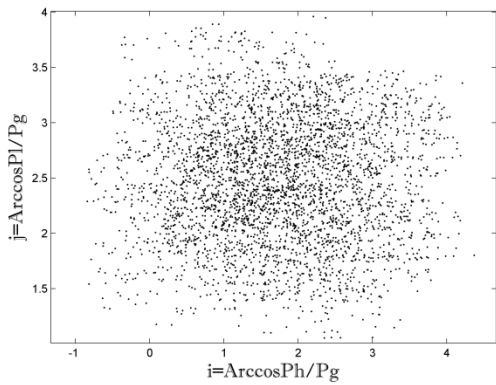


Fig. 10. Poincare section of the system in I-J plane with $\epsilon = 2 \times 10^{-8}$

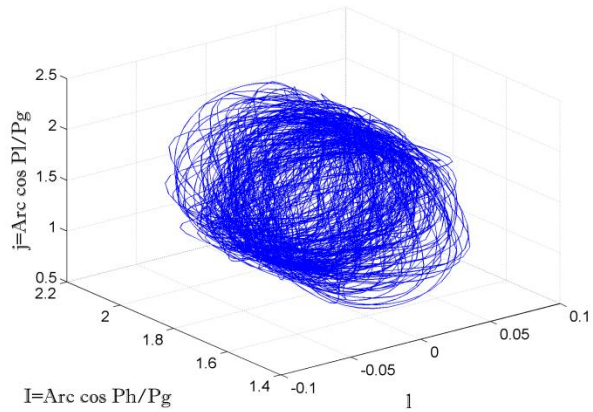


Fig. 11. Chaotic trajectory $l - I - J$ of the phase portrait of the system

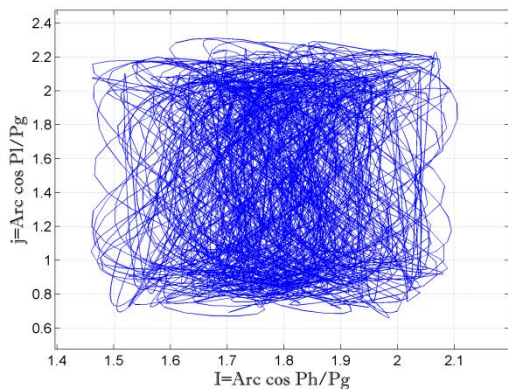


Fig. 12. Chaotic trajectory $I - J$ of the phase portrait of the system

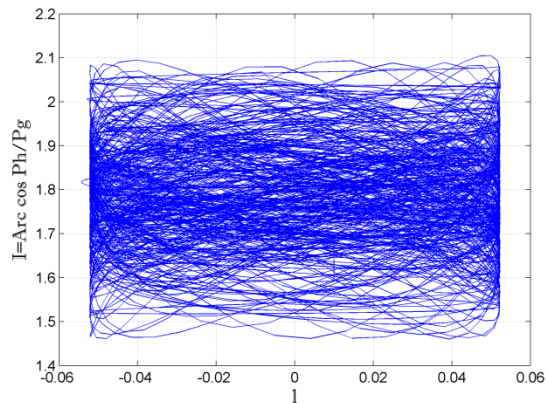


Fig. 13. Chaotic trajectory $l - I$ of the phase portrait of the system

6. Mathematical Analysis of Chaos Using Melnikov Method

In this section, chaotic dynamic and heteroclinic bifurcation is analyzed mathematically on the Roto-Translatory motion of the gyrostat system. In order to analyze the chaos mathematically, we use Melnikov method. The Melnikov method is a perturbation technique for proving the existence of intersecting heteroclinic orbits in a class of time-periodic vector field. The existence of intersection of heteroclinic orbits implies the existence of horseshoes and chaos phenomenon due to the Smale-Birkhoff theorem with the chaos appearance near the unperturbed heteroclinic orbits. The essential idea is to use the solution of the unperturbed system in studying the perturbed solution. Since the system under consideration is expressed with its perturbation equations, this method can be a proper means for chaos analysis [2-8, 24].

In order to apply the Melnikov method, particular attention is due to the equations of motion (51) through (60). Since the equations (54), (55), (59), and (60) are related to the translational motion affecting the perturbation, we use only the rotational equations of motion in the Melnikov integral and its solutions of the heteroclinic orbits.

Thus, what is important about the use of Melnikov's method is that it is capable of giving the solution of the unperturbed heteroclinic orbits usable for the perturbed system. In order to solve the unperturbed heteroclinic orbits more efficiently, it is best to write the rotational Euler equation (5) in terms of the angular momentum in the unperturbed and torque-free case. This results in the equations

$$\begin{aligned} \dot{H}_x + \frac{(I_{zz} - I_{yy})}{I_{yy}I_{zz}} H_y H_z &= 0 \\ \dot{H}_y + \frac{(I_{xx} - I_{zz})}{I_{xx}I_{zz}} H_x H_z &= 0 \\ \dot{H}_z + \frac{(I_{yy} - I_{xx})}{I_{xx}I_{yy}} H_x H_y &= 0 \end{aligned} \tag{64}$$

Equations (64) are nondimensionalized next using the parameters defined as follows. [2, 3]

$$h_i \triangleq \frac{H_i}{H_T} \quad I_1 \triangleq \frac{I_{zz}}{I_{yy}} \quad I_2 \triangleq \frac{I_{xx}}{I_{yy}} \quad (\cdot)' \triangleq \frac{I_{yy}}{H_T} (\dot{\cdot}) \quad \tau \triangleq \frac{tH_T}{I_{yy}}$$

, in which τ is the nondimensional time and H_T is the overall angular momentum of the system defines as

$$H_0^2 = H_x^2 + H_y^2 + H_z^2 + H_{R_0}^2 + H_{\omega_0}^2 \tag{65}$$

, where H_0 is constant due to the torque-free motion. The translational motion of the satellite is in the circular orbit in the unperturbed case, therefore, H_{R_0} , and H_{ω_0} are constant, and equation (65) is summarized as

$$H_T^2 = H_x^2 + H_y^2 + H_z^2 = H_0^2 - H_{R_0}^2 - H_{\omega_0}^2 \Rightarrow h^2 = h_x^2 + h_y^2 + h_z^2 \tag{66}$$

After applying the nondimensional parameters on equation (64), we have

$$\begin{aligned} h'_x + \left(\frac{1 - I_1}{I_1}\right) h_y h_z &= 0 \\ h'_y + \left(\frac{I_1 - I_2}{I_1 I_2}\right) h_x h_z &= 0 \\ h'_z + \left(\frac{I_2 - 1}{I_2}\right) h_x h_y &= 0 \end{aligned} \tag{67}$$

The energy equation of the system including kinetic and potential energy is defined as

$$E = \frac{1}{2} I_{xx} \omega_{xx}^2 + \frac{1}{2} I_{yy} \omega_{yy}^2 + \frac{1}{2} I_{zz} \omega_{zz}^2 + \frac{1}{2} m_s \dot{R}_0^2 + \frac{1}{2} (m_s R_0^2) \omega_0^2 + \frac{GMm_s}{R_0} \tag{68}$$

, where E is constant since the satellite moves in a conservative environment. Also, the terms related to the translational kinetic energy and potential energy are constant. Consequently, the energy equation is expressed as

$$\tilde{T} = \frac{h_x^2}{I_2} + h_y^2 + \frac{h_z^2}{I_1} \tag{69}$$

, where, \tilde{T} is the nondimensional kinetic energy defined as $\tilde{T} \triangleq \frac{2I_{yy}T}{H^2}$ in which T is the kinetic energy of the system. The spherical phase portrait for the unperturbed system is demonstrated in Fig. 14 showing the hyperbolic saddle point and heteroclinic orbits. Any trajectory on the momentum sphere defined in equation (66) is determined by the intersection of the momentum sphere and the energy ellipsoid defined in equation (69) in the body coordinates. The angular momentum vector always remains on a particular intersection of the momentum sphere and energy ellipsoid. The sphere radius is $h = 1$ and must lie between the smallest and largest semi axes of the ellipsoid.

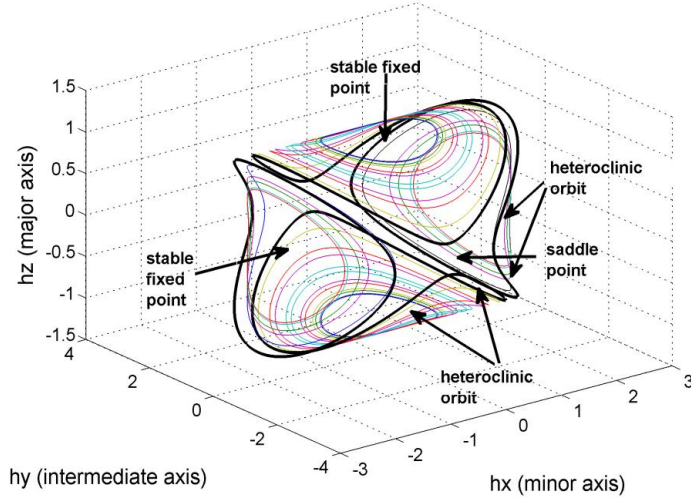


Fig. 14. Momentum sphere of the system with the heteroclinic orbits and hyperbolic saddle points

Since, $I_{xx} > I_{yy} > I_{zz}$ or as dimensionless $I_2 > 1 > I_1 > 0$, the condition on the radius of sphere is given by $I_1\tilde{T} < 1 < I_2\tilde{T}$. Also, the heteroclinic orbits are formed when the momentum sphere and energy ellipsoid are tangent at the saddle point $(0, \pm 1, 0)$, as shown by equation (67). Therefore, the energy level for the heteroclinic orbits must be given as $\tilde{T} = 1$ or $T = H^2/2I_{yy}$. According to the above explanation and using equations (66), (67), and (69), the solution of the angular momentum along the heteroclinic orbits is given by [1, 5-8]

$$\begin{aligned} h_x &= \pm \left(\frac{I_2(1 - I_1)}{I_2 - I_1} \right)^{\frac{1}{2}} \operatorname{sech}(N\tau) \\ h_y &= \pm \tanh(N\tau) \\ h_z &= \pm \left(\frac{I_1(I_2 - 1)}{I_2 - I_1} \right)^{\frac{1}{2}} \operatorname{sech}(N\tau) \end{aligned} \quad (70)$$

, where, $N = \sqrt{(I_1 - 1)(1 - I_2)/I_1 I_2}$ and $\tau = 0$ is chosen to eliminate constants of integration and the appropriate signs are chosen to give the four heteroclinic trajectories around the saddle point. Now, based on the Serret-Andoyer relations, the solution of the heteroclinic orbits in equation (70) is transformed by the Deprit variables, leading to equations (71) below, which are similar to the spherical coordinates in its overall structure. [6]

$$\begin{aligned} h_x &= P_g \sin J \sin l = \pm \left(\frac{I_2(1 - I_1)}{I_2 - I_1} \right)^{\frac{1}{2}} \operatorname{sech}(N\tau) \\ h_y &= P_g \sin J \cos l = \pm \tanh(N\tau) \\ h_z &= P_g \cos J = \pm \left(\frac{I_1(I_2 - 1)}{I_2 - I_1} \right)^{\frac{1}{2}} \operatorname{sech}(N\tau) \end{aligned} \quad (71)$$

On the other hand, based on the equations (51) to (60) in the unperturbed case, the states $h, \lambda_0, r_0, P_h, P_g, P_{\lambda_0}, P_{r_0}$ and I are constant and the states l, P_l , and J are determined from the solutions of heteroclinic orbits and equations (71). Therefore,

$$\cos l = \sqrt{\frac{I_2(1 - I_1)}{I_1(I_2 - 1)}} \operatorname{csch}(N\tau) \tag{72}$$

$$\cos J = \operatorname{sech}(N\tau) \tag{73}$$

Since P_g is constant and for values of I_{yy} near the I_{xx} , g is estimated by equation (52) by $g \cong \Omega\tau$. Accordingly, the equations of motion of the system are rewritten for the perturbed system to be used in the Melnikov integral. Hence,

$$\dot{l} = F_{l1} + \varepsilon(G_{l1}) \tag{74}$$

$$\dot{P}_l = F_{l2} + \varepsilon(G_{l2}) \tag{75}$$

$$\dot{g} = F_{g1} + \varepsilon(G_{g1}) \tag{76}$$

$$\dot{P}_g = F_{g2} + \varepsilon(G_{g2}) \tag{77}$$

, where $\varepsilon = \frac{1}{r_0^2}$ and,

$$F_{l1} = P_l \left(\frac{1}{I_{zz}} - \frac{S_l^2}{I_{xx}} - \frac{C_l^2}{I_{yy}} \right)$$

$$G_{l1} = \frac{1}{m_s} \{S_l^2 S_j + S_l S_g S_l\}$$

$$F_{l2} = -(P_g^2 - P_l^2) S_l C_l \left(\frac{1}{I_{xx}} - \frac{1}{I_{yy}} \right)$$

$$G_{l2} = v_0^2 \left\{ \frac{1}{2} (I_{xx} - I_{yy}) C_l S_l S_l \right\} + \frac{1}{m_s} \{S_g S_l - P_l S_l S_g C_l\} + \frac{2\mu}{3r_0} \{S_h S_g C_l^2 - 2S_j C_l C_h^2\}$$

$$F_{g1} = P_g \left(\frac{S_l^2}{I_{xx}} + \frac{C_l^2}{I_{yy}} \right)$$

$$G_{g1} = 0$$

$$F_{g2} = 0$$

$$G_{g2} = v_0^2 \left\{ -I_{zz} S_l^2 S_j^2 S_g C_g + \frac{1}{2} (I_{xx} - I_{yy}) S_l^2 S_j S_g - \frac{1}{2} I_{yy} C_l^2 C_g \right\} + \frac{1}{m_s} \{-P_l (S_l C_g S_l) - C_g C_l\} + \frac{2\mu}{3r_0} \{(I_{zz} - I_{xx})(-S_l C_l C_h^2 + C_j S_l^2)\}$$

Then the Melnikov function can be written in the integral form of

$$M(\tau_0) = \int_{-\infty}^{+\infty} F(q_0(t)) \wedge G(q_0(t), t + t_0) dt \tag{78}$$

, where F is a Hamiltonian vector field and $G(x, t)$ is a small perturbation, $q_0(t)$ is the solution of the heteroclinic orbits in the unperturbed system, and the symbol \wedge is the wedge operator defined by $(a \wedge b = a_1 b_2 - a_2 b_1)$.

Substituting equations (74-77) into equation (78) yields

$$M(\tau_0) = \int_{-\infty}^{+\infty} \{F_{l1} G_{l2}(t + t_0) - F_{l2} G_{l1}(t + t_0)\} dt + \int_{-\infty}^{+\infty} \{F_{g1} G_{g2}(t + t_0) - F_{g2} G_{g1}(t + t_0)\} dt \tag{79}$$

After solving the above integral using integral tables, integration by parts, Cauchy's integral, and residue theory, the Melnikov function is derived as [27]

$$M(\tau_0) = C_1 + C_2 \sin(\Omega\tau_0) + C_3 \cos(\Omega\tau_0) + C_4 \sin(2\Omega\tau_0) \tag{80}$$

, in which

$$\begin{aligned}
 C_1 &= \frac{3\mu}{4NR_0A} \left\{ \frac{I_1 - I_2}{I_2} + I_1(1 - I_2) \right\} \\
 C_2 &= \frac{I_2(I_1 - 1)\pi\Omega}{I_1(I_2 - 1)m_s I_{yy}} + \operatorname{sech} \left(\frac{\pi\Omega}{2N} \right) \left\{ \left(\frac{\pi}{I_{yy}m_s N} \right) \left(\frac{-I_2^2 + 2I_2 - I_1}{I_1 I_2 (I_2 - 1)} \right) + \frac{3\pi\mu(I_2 - 1)}{16r_0 N} \left(\frac{(I_1 + I_2 + I_1 I_2)\{I_1(I_2 - 1)\}^{\frac{1}{4}}}{I_1 I_2 (I_2 - I_1)^{\frac{1}{4}}} \right) \right. \\
 &\quad \left. + \left(\frac{1}{I_2} - 1 \right) \left(\frac{I_2 - I_1}{I_1(I_2 - 1)} \right)^{\frac{1}{4}} \right\} + \operatorname{tanh} \left(\frac{\pi\Omega}{2N} \right) \left\{ \frac{\sqrt{I_2(1 - I_1)(I_2 - I_1)}}{I_1(I_2 - 1)} \left(\frac{1}{I_2} - 1 + \frac{I_1(I_2 - 1)}{I_2 - I_1} \right) \left(\frac{\pi}{m_s I_{yy} N} \right) \right\} \\
 C_3 &= \operatorname{sech} \left(\frac{\pi\Omega}{2N} \right) \left\{ \left(\frac{\pi\Omega B}{2I_{yy}m_s N^2} \right) \left(\frac{I_1 - 2I_1 A^2}{2I_1 I_2 A} + \frac{1}{A} - \frac{1}{AI_2} \right) + \left(-\frac{v_0^2}{4N} - \frac{\pi}{2Nm_s I_{yy}} \right) \left(\frac{1 + I_1 A^2 - I_1}{I_1 A} \right) \right\} \\
 &\quad + \operatorname{tanh} \left(\frac{\pi\Omega}{2N} \right) \left\{ \left(\frac{\pi B}{2I_{yy}m_s N} \right) \left(\frac{2I_1 A^2 - I_2}{2I_1 I_2 A} \right) \right\} \\
 C_4 &= \frac{v_0^2}{8\Omega} \left(\frac{I_2 - I_1 I_2 A^3 - I_1 I_2 A}{I_1 A^2} \right)
 \end{aligned}$$

, where $A = \sqrt{\frac{I_1(I_2-1)}{I_2-I_1}}$ and $B = \sqrt{\frac{I_2(1-I_1)}{I_2-I_1}}$.

Equation (80) can be written in a simpler form as

$$M(\tau_0) = C_1 + C_5 \sin(\Omega\tau_0 + \phi) + C_4 \sin(2\Omega\tau_0) \quad (81)$$

, with $C_5 = \sqrt{C_2 + C_3}$ and $\phi = \operatorname{Arctan}\left(\frac{C_3}{C_2}\right)$.

According to equation (81), it has Zero-Crossing if,

$$|C_4| + |C_5| > C_1 \quad (82)$$

This indicates the transversality in the heteroclinic orbits and a possible chaos in the system. Based on the values of the system parameters in the simulation in the previous section, condition (82) is in fact satisfied, and the Melnikov method mathematically proves the chaotic behavior in the system. Furthermore, if

$$C_4 + C_5 < C_1 \quad (83)$$

, then (81) has no Zero-Crossing and the system is definitely not chaotic. Therefore, we can design the parameters of the system based on satisfying condition (83), and as a result, the incidence of chaos in the system can be prevented.

7. Conclusion

This work considers the modeling and chaos analysis of the Roto-translatory motion of a gyrostatt satellite with three reaction wheel stabilizers under the gravity gradient torques. In order to derive the dynamic model of the system, coupled Newton-Euler equations is initially modeled. However, the complexity inherent in the coupled spin-orbit equations is a strong incentive to reduce the order of the system model. Therefore, the dynamics of the system is re-derived using the Hamiltonian approach. The developed canonical Deprit transformation with the new Serret-Andoyer variables reduced the system with five degrees of freedom to a system with three degrees of freedom, rendering it possible to perform a thorough, yet less laborious nonlinear analysis of the system. Simulation results of the reduced system consisting of the phase space trajectories and Poincare section demonstrate the heteroclinic bifurcation in the system. The existence of intersecting heteroclinic orbits then implies the existence of horseshoe and chaos based on the Smale-Birkhoff Theorem. In addition, the Lyapunov exponent satisfies numerically the chaos phenomenon in the perturbed system. On the other hand, the Melnikov method can be an appropriate means for the analysis of chaotic systems when the model of the system is derived as a perturbed Hamiltonian system. Therefore, according to the results obtained from Melnikov function, the intersection of stable and unstable manifolds in the heteroclinic orbits is verified and the chaos and heteroclinic bifurcation is mathematically demonstrated. Consequently, the bounds on the values of

the design parameters can be determined for the system such that the system does not fall in a state of chaos in the absence of a control system.

8. Appendix A: Deriving the total angular momentum

In order to proving of equation (2), the total angular momentum of the Gyrostat satellite with respect to G is as

$$\vec{H}_T = \vec{H}_{B,G} + \sum_{i=1}^3 \vec{H}_{i,G} \quad (\text{A.1})$$

, where $\vec{H}_{B,G}$ is the angular momentum of the main body relative to G , that is derived as

$$\vec{H}_{B,G} = \vec{H}_{B,G_B} + (\vec{\rho} \times m_B \vec{V}_{G_B}) \quad (\text{A.2})$$

, where \vec{H}_{B,G_B} is the angular momentum of the main body with respect to G_B , $\vec{\rho}$ is the vector $\overrightarrow{GG_B}$, and \vec{V}_{G_B} is the velocity of the G_B . Furthermore, $\vec{H}_{i,G}$ is the angular momentum of each gyro relative to G and it is derived as follows.

$$\vec{H}_{i,G} = \vec{H}_{i,G_i} + (\vec{\rho}_i \times m_g \vec{V}_{G_i}) \quad i = 1,2,3 \quad (\text{A.3})$$

, where \vec{H}_{i,G_i} is the angular momentum of the each gyro relative to G_i , $\vec{\rho}_i$ is the vector $\overrightarrow{GG_i}$, and \vec{V}_{G_i} is the velocity of the G_i . Substituting equations (A.2) and (A.3) into Eq. (A.1) and placing the center of coordinate system in G , the total angular momentum of the system is derived as follows.

$$\begin{aligned} \vec{H}_T = & [(I_x + 3I_W)\omega_{xx} + I_W\Omega_x]\hat{i} + [(I_y + 3I_W)\omega_{yy} + I_W\Omega_y]\hat{j} + [(I_z + 3I_W)\omega_{zz} + I_W\Omega_z]\hat{k} \\ & + \{\vec{\rho} \times m_B(\vec{\omega}_T \times \vec{\rho})\} + \left\{ \sum_{i=1}^3 \vec{\rho}_i \times m_g(\vec{\omega}_T \times \vec{\rho}_i) \right\} \end{aligned} \quad (\text{A.4})$$

Then, using the vector triple product formulae as $\vec{\rho} \times (\vec{\omega}_T \times \vec{\rho}) = (\vec{\rho} \cdot \vec{\rho})\vec{\omega}_T - (\vec{\rho} \cdot \vec{\omega}_T)\vec{\rho}$ in equation (A.4), where $\vec{\omega}_T$ is the total angular velocity of the Gyrostat based on equations (3), and simplifying these relations, ultimately equation (A.4) results equation (2).

References

- [1] G. L. Gray, D. C. Kammer, I. Dobson, A. J. Miller, 'Heteroclinic Bifurcation in Rigid Bodies Containing Internally Moving Parts and a Viscous damper', ASME Transaction, 66 (1999) 720-728.
- [2] Y. Baozeng, X. Jiafang, Chaotic attitude maneuvers in spacecraft with a completely liquid-filled cavity, Journal of Sound and Vibration, 302 (2007) 643-656.
- [3] Y. Baozeng, Heteroclinic bifurcations in completely liquid-filled spacecraft with flexible appendage, Nonlinear Dynamics, 51 (2008) 317-327.
- [4] L. Zhou, Y. Chen, F. Chen, Stability and chaos of a damped satellite partially filled with liquid, Acta Astronautica, 65 (2009) 1628-1638.
- [5] X. Tong, B. Tabarrok, F. P. J. Rimrott, Chaotic Motion of an Asymmetric Gyrostat in the Gravitational Field, International Journal of Non-Linear Mechanics, 30 (1995) 191-203.
- [6] J. Kuang, S. Tan, K. Arichandran, A.Y.T. Leung, Chaotic dynamics of an asymmetrical gyrostat, International Journal of Non-Linear Mechanics 36 (2001) 1213-1233.
- [7] J. Kuang, A.Y.T. Leung, S. Tan, Hamiltonian and chaotic attitude dynamics of an orbiting gyrostat satellite under gravity-gradient torques, Physica D, 186 (2003) 1-19.
- [8] J.L. Kuang, P.A. Meehan, A.Y.T. Leung, on the chaotic rotation of a liquid-filled gyrostat via the Melnikov-Holmes-Marsden integral, International Journal of Non-Linear Mechanics, 41 (2006) 475-490.
- [9] K. H. Shirazi, M. H. Ghaffari-Saadat, Chaotic motion in a class of asymmetrical Kelvin type gyrostat satellite, International Journal of Non-Linear Mechanics, 39 (2004) 785-793.
- [10] K.H. Shirazi, M.H. Ghaffari-Saadat, " Bifurcation and Chaos in an Apparent-Type Gyrostat Satellite", Nonlinear Dynamics, 39, 259-274, 2005
- [11] A. Elipe, V. Lanchares, Exact solution of a triaxial gyrostat with one rotor, Celestial Mechanics and Dynamic Astronomy, 101 (2008) 49-68.
- [12] A. V. Doroshin, Analysis of attitude motion evolutions of variable mass gyrostats and coaxial rigid bodies system, International Journal of Non-Linear Mechanics, 45 (2010) 193-205.

- [13] A. Celletti, L. Chierchia, Hamiltonian Stability of Spin–Orbit Resonances in Celestial Mechanics, *Celestial Mechanics and Dynamical Astronomy*, 76 (2000) 229–240.
- [14] A. Celletti, L. Chierchia, Measures of basins of attraction in spin-orbit dynamics, *Celestial Mechanics and Dynamical Astronomy*, 101 (2008) 159–170.
- [15] J. F. Palacián, Dynamics of a satellite orbiting a planet with an inhomogeneous gravitational field, *Celestial Mechanics and Dynamical Astronomy*, 98 (2007) 219–249.
- [16] P. Gurfil, A. Elipe, W. Tangren, M. Efroimsky, the Serret–Andoyer Formalism in Rigid-Body Dynamics: I. Symmetries and Perturbations, *Regular and Chaotic Dynamics*, 12 (2007) 389–425.
- [17] M. H. Andoyer, *Course de Mecanique Celeste*, Gauthier Villars, Paris, 1923.
- [18] Sadov S., Computation of Quasi periodic Fundamental Solution of Helmholtz Equation, *Gordon and Breach*, 1 (1997) 551–558.
- [19] Inarrea M., Chaos and its control in the pitch motion of an asymmetric magnetic spacecraft in polar elliptic orbit, *Chaos Solitons and Fractals* 40 (2009) 1637–1652.
- [20] J. Kuang, P. A. Meehan, A.Y.T. Leung, S. Tan, Nonlinear dynamics of a satellite with deployable solar panel arrays, *International Journal of Non-Linear Mechanics* 39 (2004) 1161–1179.
- [21] Y. Z. Liu, H. J. Yua, L. Chen, Chaotic attitude motion and its control of spacecraft in elliptic orbit and geomagnetic, *Acta Astronautica* 55 (2004) 487–494.
- [22] P. A. Meehan, K. J. Austin, Prediction of chaotic instabilities in a dragline bucket swing, *International Journal of Non-Linear Mechanics* 41 (2006) 304–312.
- [23] R. Hilborn, *Chaos and Nonlinear Dynamics: An Introduction for Scientists and Engineers*, Oxford University press, New York, 2000.
- [24] S. Wiggins, *Introduction to Applied Nonlinear Dynamical Systems and Chaos*, Springer-Verlag, New York, 2003.
- [25] M. J. Sidi, *Spacecraft Dynamics and Control: A Practical Engineering Approach*, Cambridge University Press, 1997.
- [26] J. R. Wertz, *Spacecraft Attitude Determination and Control*, Kluwer Academic Publishers, London, 1990.
- [27] M. Spiegel, S. Lipschutz, J. Liu, *Mathematical Handbook of Formulas and Tables*, McGraw-Hill Professional, 1999.